# Line parameter study of ozone at 5 and 10$\mu$m using atmospheric FTIR spectra from the ground: A spectroscopic database and wavelength region comparison

Christof Janssen, Corinne Boursier, Pascal Jeseck, Yao Té

# Line parameter study of ozone at 5 and 10 μm using atmospheric FTIR spectra from the ground: A spectroscopic database and wavelength region comparison

Christof Janssen[a,*], Corinne Boursier[a], Pascal Jeseck[a], Yao Té[a]

[a]*LERMA-IPSL, Sorbonne Universités, UPMC Univ Paris 6, Observatoire de Paris, PSL Research University, CNRS, F-75005, Paris, France*

**Abstract**

Atmospheric ozone concentration measurements mostly depend on spectroscopic methods that cover different spectral regions. Despite long years of measurement efforts, the uncertainty goal of 1% in absolute line intensities has not been reached yet. Multispectral inter-comparisons using both laboratory and atmospheric studies reveal that important discrepancies exist when ozone columns are retrieved in different spectral regions. Here, we use ground based FTIR to study the sensitivity of ozone columns on different spectroscopic parameters as a function of individual bands for identifying necessary improvements of the spectroscopic databases. In particular, we examine the degree of consistency that can be reached in ozone retrievals using spectral windows in the 5 and 10 μm bands of ozone. Based on the atmospheric spectra, a detailed database inter-comparison between HITRAN (version 2012), GEISA (version 2011) and S&MPO (as retrieved from the website at the end of 2015) is made. Data from the 10 μm window are consistent to better than 1%, but there are larger differences when the windows at 5 μm are included. The 5 μm results agree with the results from 10 μm within ±2 % for all databases. Recent S&MPO data are even more consistent with the desired level of 1 %, but spectroscopic data from HITRAN give about 4% higher ozone columns than those from GEISA. If four sub-windows in the 5 μm band are checked for

*corresponding author
*Email address:* christof.janssen@upmc.fr (Christof Janssen)

consistency, retrievals using GEISA or S&MPO parameters show less dispersion than those using HITRAN, where one window in the *P*-branch of the $\nu_1 + \nu_3$ band gives about 2 % lower results than the other three. The atmospheric observations are corroborated by a direct comparison of the spectroscopic databases, using a simple statistical analysis based on intensity weighted spectroscopic parameters. The bias introduced by the weighted average approach is investigated and it is negligible if relative differences between databases do not correlate with line intensities. This is the case for the comparison of HITRAN with GEISA in the 10 μm region and the agreement between the simple analysis and the full retrieval is better than 0.1%. At 5 μm biases might be as high as 1.4 %, and the proposed method is thus limited to the same level of accuracy. Implications of the new data for database improvements and further studies, in particular in the 5 μm region, are discussed.

*Keywords:* ozone, atmospheric composition, remote sensing, FTIR, MIR, spectroscopic database

## 1. Introduction

The triatomic allotrope of oxygen, ozone ($O_3$), is a key molecule in Earths atmosphere. As precursor molecule for atmospheric radicals ($NO_3$, OH) it plays a central role in atmospheric oxidation. Ozone also filters harmful solar ultraviolet (UV) radiation and thus is crucial to the evolution of life as we know it. The molecule has direct impact on air quality, agricultural productivity, and the ecosystem with corresponding economic consequences. Accurate and traceable concentration measurements of this molecule thus are a priority for health and air quality authorities as well as for atmospheric and climate scientists, which has made ozone one of the key themes of dedicated global atmospheric observation programs, such as IGACO-O3/UV. [1]

[1] Integrated Global Atmospheric Chemistry Observations for ozone and UV as part of the Global Atmospheric Watch (GAW) Programme of the World Meteorological Organisation for providing reliable scientific data and information on the chemical composition of the atmosphere, its natural and anthropogenic change, and helping to improve the understanding of interactions between the atmosphere, the oceans and the biosphere.

Due to its high reactivity and the impossibility to prepare a stable reference standard along with the fact that ozone has rich and strong absorption features covering all spectral regions from the far IR to the UV, $O_3$ concentration measurements are commonly based on spectroscopic methods. These measurements thus depend on the molecular spectroscopic constants describing the interaction with light, which have to be determined experimentally. Indeed, the recommended primary method for in-situ ozone measurements in ambient air hinges on the absorption cross section in the Hartley band at 253.65 nm, whose actually recommended value suffers from a relative uncertainty of 2.1 % (at the 95 % level of confidence) [1]. In view of the need for reliable long term measurements of ozone changes of a few percent per decade [2–5], traceable spectroscopic data with a much lower level of uncertainty are desired and redeterminations of this cross section value are thus under way [6–8]. A target uncertainty for concentration measurements and remote sensing of atmospheric ozone is one percent [1, 7, 9, 10], or below. This would also allow meaningful retrieval of tropospheric ozone from satellite data where the total column is dominated by the stratospheric contribution ($\sim$ 90 %). Achieving and well characterizing this level of uncertainty will also make an important contribution to the United Nations effort in documenting long-term ozone trends [11].

In order to harmonize the spectroscopic data on ozone, the most recent mid-IR intensity studies in the 10 µm range [2–5, 12–15] have been critically reviewed [16] and the databases have been updated concordantly after 2004 [17–19]. Because three of four recent measurements showed a dispersion of just ±0.8%, it was recommended to reduce the database values by roughly 4 % which corresponded to the average of the three consistent data sets. The recommendation thus has effectively ignored the recent measurement of Smith et al. [12] even though it was consistent with previous measurements and the actual recommendation (HITRAN 2000) at that time and this was done without pointing out why this particular measurement should be less reliable than the other studies.

Interestingly, recent direct UV (300-315 nm) - IR (10 µm) inter-comparison measurements in the laboratory [20, 21], in the atmosphere from ground [22] or using satellite instruments [23] have questioned the thus obtained consistency of the updated spectroscopic parameters: using either of the two spectral regions, inter-comparisons

often find a difference of about 4 % in the derived ozone concentrations or columns. This could possibly indicate that the original HITRAN 2000 database [24] values are more consistent with recommended UV data. A similar difference of (3.6 ± 1.0) % has been found in another UV - IR inter-comparison based on simultaneous measurements at the Hg emission line at 253.65 nm and around 1133.5 $cm^{-1}$ in the $\nu_1$ band [25]. Moreover, using the same two databases (HITRAN 2004 or 2008), the ACE-FTS mission team has decided to neglect the results from ozone spectroscopic data in the 5 μm band (in the $\nu_1+\nu_2$ band around 1800 $cm^{-1}$ and in the $\nu_1+\nu_3$ band around 2100 $cm^{-1}$), because of apparent discrepancies with the results obtained from retrieval in the 10 μm fundamental region [23]. This has triggered another inter-comparison study [26] between the integrated absorption in the Chappuis band (515 - 715 nm) and the $\nu_1+\nu_3$ combination band. There, however, no inconsistencies in recommended databases have been found, but optical densities in the visible were very weak though (< 4 %). Thomas et al. [27] studied recently possible inconsistencies between the 5 and 10 μm regions by absolute measurements in each of these two regions. Their results at 10 μm are compatible with the 2004 or 2008 HITRAN databases and about 2 % lower than the actual databases in the 5 μm region, which, if significant, could even increase the observed discrepancy in the satellite data [23, 28].

Very recently, the first direct inter-comparison between the 3 and 10 μm as well as the 4 and 10 μm regions has been published [29]. This study is based on ground based FTIR solar absorption spectra and systematic differences of up to 7 % between the different regions have been revealed, most likely due to inconsistencies in the spectroscopic data.

Given these many seemingly conflicting results, further inter-comparisons, ideally using identical conditions for the ozone concentration and the optical light path, are sought for. Besides of the inherent difficulty to prepare ozone for comparison and absolute intensity measurements, some of the discrepancies are certainly due to the use of different lines and spectral regions. In this article we thus try to investigate the consistency of the 5 μm data with the 10 μm region: i) globally, as a function of the vibrational band and ii) locally, as a function of few individual transitions, using atmospheric observations from a ground based FTIR instrument. The present study

thus is part of a greater effort of using ground based atmospheric remote sensing studies for improving the spectroscopic databases, such as has been demonstrated for the case of water [30], for example.

Our comparisons are done using the currently available data from the three different spectroscopic databases GEISA [31], HITRAN [32] and S&MPO [33], which allows one to investigate differences and possible inconsistencies. Due to the complexity of linking column measurements to spectroscopic data, a simple method is introduced that permits to derive characteristic spectroscopic parameters for each spectral window and database. Based on comparisons of these representative values, differences in atmospheric retrievals can be traced back to differences in the spectroscopic databases. The comparison of databases in each of the spectral regions is thus another goal of this article, which is structured as follows: We begin with a description of the experimental tools, the spectroscopic data and the retrieval procedure. The sensitivity of ozone columns on different spectroscopic parameters in the 10 μm range is then discussed and we conclude with a detailed comparison of ozone data in the spectroscopic databases in the light of our measurements.

## 2. Experimental setup and data

### *2.1. Observation site and instrumental description*

Atmospheric observations were performed using the Paris ground-based Fourier transform spectrometer (FTS-Paris). This instrument is operated by the SMILE/LERMA[2] team and is part of the QualAir air quality research station of Université Pierre et Marie Curie (UPMC). The instrument is located in downtown Paris on the UPMC campus (48°50'N, 2°21'E at 65 m a.s.l). A detailed description of the system can be found elsewhere [34]. Here, we just give a short description and technical key data are summarized in Table 1.

[2]SMILE is the French acronym for "*M*olecular *S*pectroscopy and *L*aser *I*nstrumentation for the *E*nvironment"

### 2.2. Data acquisition

The spectra recorded by ground-based FTIR contain rovibrational signatures of atmospheric species in the characteristic fingerprint and group frequency regions (3 – 10 μm, extendable). To optimize the signal-to-noise ratio in the spectral domains of the ozone signals, appropriate combinations of optical filters and detectors have been chosen (see Table 1). Data were acquired during daytime and only clear sky spectra have been kept for the analysis. In order to optimize the signal-to-noise ratio, the evaluation has further been restricted to spectra that were obtained around noon (10:00 – 14:00). Here we present data that were acquired at six days in 2013. An overview of the spectroscopic data and windows is given in Figure 1.

### 2.3. Spectroscopic Data

Data were taken from the latest versions of the three databases GEISA, HITRAN and S&MPO (G11, H12 and S15, hereafter). The origin of these data and the available parameters are specified for each spectral region separately. Note that S&MPO does not keep track of changes of the available data. The data used here represent a snapshot made in December 2015 using the `smpo.univ-reims.fr` website. All of the databases essentially provide spectroscopic data concerning the main and singly substituted ozone species: $^{16}O_3$, $^{16}O^{16}O^{18}O$, $^{16}O^{18}O^{16}O$, $^{16}O^{16}O^{17}O$, $^{16}O^{17}O^{16}$ (or 666, 668, 686, 667, 676 in shorthand notation). While the singly substituted isotopologues except for $^{16}O^{18}O^{16}O$ have been included into the database only at the end of 2015, S15 also includes the pure $^{18}O_3$ isotopologue and gives intensities on a per species' basis. H12 and G11 assume that the above molecules occur in fixed proportions of 0.992901, 0.00398194, 0.00199097, 0.000734 and 0.00370 respectively [24]. These relative abundance factors are therefore already incorporated into intensities given in the databases [35], which is also the convention assumed by the retrieval software. The above relative values are based on the isotope abundance of standard mean ocean water (SMOW) [36]. By taking these proportions one evidently ignores the strong and variable isotopic enrichments that actually occur in atmospheric ozone [37–39]. Nevertheless, the assumption is made throughout and will have no significant impact on the total ozone column values.

Another notable difference between databases is the kind of spectroscopic parameters that are provided. Table 2 gives a comparison of these data. The lack of the air temperature coefficient $n_{\mathrm{air}}$ of the broadened half width in S&MPO needs to be pointed out here as a possible obstacle for atmospheric applications. Throughout the paper we have assumed the constant value $n_{\mathrm{air}} = 0.76$ in doing retrievals with S15. As far as line intensities of $^{16}O_3$ are concerned, data from the $\{\nu_1, \nu_3\}$ fundamentals at 10 µm in H12 and S15 are due to dipole moments of Flaud *et al.* [16] (see Ref. [40]), while corresponding values in G11 are referenced to Ref. [14]. The 5 µm cold band transitions of $^{16}O_3$ in H12 stem from the calulation published in Ref. [41] and are scaled by a normalization factor of $1/(1.04)$ [40]. The same data in G11 result from the work in Ref. [42], while corresponding transitions in S15 come from calculations of GSMA in Reims [43].

The 10 µm region comprises the fundamental of the dyad formed by the normal stretch modes $\nu_1$ and $\nu_3$, but also harmonic and hot band transitions. We note that normal mode frequencies are 1103.08 and 1041.89 $\mathrm{cm}^{-1}$ for $\nu_1$ and $\nu_3$, respectively and that the $\nu_3$ band has the highest band intensity of the normal modes. Altogether 1157 lines in the selected window 10–1 at and above our threshold intensity of $10^{-23}$ cm are reported in HITRAN.

The threshold, which was not applied to the retrieval that included all available lines in the databases, corresponds to 2 to 3 times our limit of detection (LOD). These lines belong to different vibrational transitions. Using the Boltzmann factors

$$F_{\mathrm{B}}(T) = \exp\left(-c_2 E''/T\right), \tag{1}$$

defined by the lower state energy $E''$, temperature $T$ and second radiation constant $c_2 = 1.4387770(13)\,\mathrm{K\ cm}^1$, one readily estimates that only ground state $\{001, 100\} \leftarrow 000$ and hot band transitions from the first excited states 010, 001 and 100 need to be considered at 296 K, if contributions of less than 0.2 % to the total intensity are neglected. The restriction to the above transitions should even be more accurate, because temperatures in the ozone layer are much lower.

155 *2.3.1. Retrieval strategy*

Ozone total columns

$$C_{O_3} = \int n_{O_3}(z)\, dz \tag{2}$$

where $n_{O_3}(z)$ is the ozone number density along the light path with coordinate $z$, are retrieved using the PROFILE FIT (PROFFIT) algorithm developed by Hase et al. [44]. The radiative algorithm (forward model) is based on the Beer-Lambert law and calcu-
160 lates the atmospheric absorbance, which is compared and fitted to the measured spectrum using a least squares minimization method. Input parameters for the forward modeling are: spectroscopic line parameters (position, intensity, pressure line shift, pressure broadening parameters) from the spectroscopic databases; atmospheric pressure and temperature vertical profiles from NOAA (see http://www.ncep.noaa.gov); a
165 priori vertical Volume Mixing Ratio (VMR) profiles of all of the studied species, the $H_2O$ continuum [45], and the instrument line shape [46–48], which is regularly monitored using sealed and non-sealed gas cells filled with HCl, HBr and $N_2O$. The inversion model supports both optimal estimation and Twomey-Tikhonov constraints and is able to perform the retrieval in log(VMR) space for strong variability in an optimal
170 manner. Columns are measured along the light path but are usually converted to vertical columns, assuming spherical symmetry of the atmosphere. In this paper we do not need to be concerned with the difference between these two and might for simplicity assume that the absorption occurs along the vertical direction.

In the spectral regions corresponding to the fundamental $\{\nu_1, \nu_3\}$ bands at 10 µm,
175 one window (10−1) consisting out of 5 sub-windows was used and in the region of the $\nu_1 + \nu_3$ combination bands at 5 µm four different windows (5−1 through 5−4) with between 4 and 7 sub or micro-windows were employed in the analysis. The windows and the micro-windows are detailed in Table 3 and Figure 2 gives a graphical representation of the acquired spectra. Micro-windows in both spectral ranges were chosen
180 in order to minimizing contributions from interfering species, which mainly are $H_2O$, $CO_2$, $N_2O$, CO and OCS. Their contributions were determined in separate retrievals using appropriate spectral windows. The ozone columns have then be retrieved using a daily mean vertical profile of the interferer substances.

We note that the 10 µm range has been used intensively for the retrieval of ozone in both space missions (for instance MIPAS [49] and IASI [22]) and ground based remote sensing (NDACC [4, 50]). $O_3$ columns retrieved from window 10-1 are therefore considered as reference values.

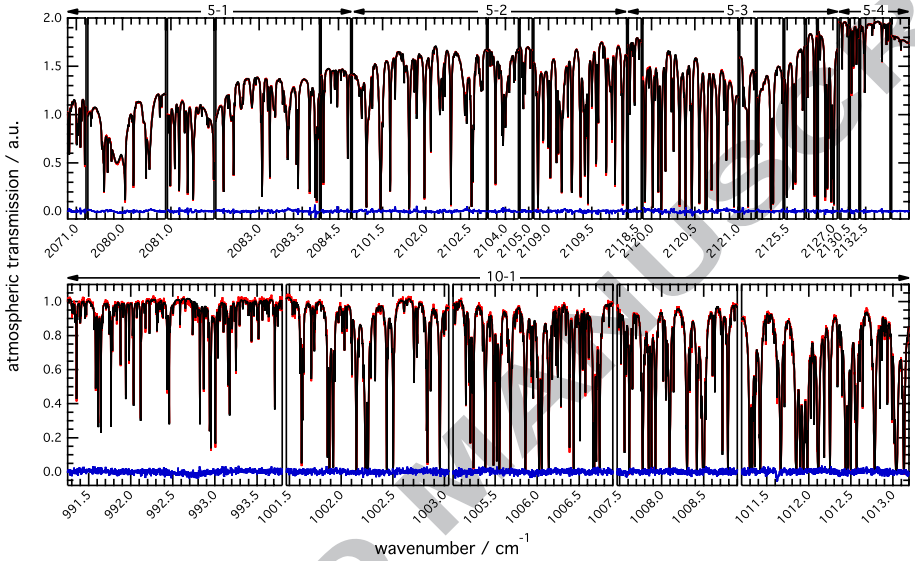


Figure 1: Overview of spectral regions and micro-windows used for the ozone retrieval. Top – 5 µm windows, bottom – 10 µm window. Red, black and blue traces respectively indicate measured and fitted spectrum as well as the residual signal. See Table 3 for micro-window boundaries and supplemental information.

## 3. Parameter Sensitivity Study

### *3.1. Atmospheric conditions*

Figure 2 gives an overview of the typical retrieved ozone profile and atmospheric measurement conditions. In the altitude range from 0 to 34 km, ozone number densities vary between 0.9 and $4 \cdot 10^{12}$ cm$^{-3}$, with the maximum reached at circa 23 km of altitude. Above 34 km, ozone concentrations decrease exponentially at a rate of about one decade per 7 km. Temperatures at the ozone maximum are on the order of 220 K and the column averaged ozone temperature

$$\overline{T}_{O_3} = \frac{\int dz\, T(z)\, n_{O_3}(z)}{\int dz\, n_{O_3}(z)} \tag{3}$$

takes the value of 235 K. Most of the ozone signal thus comes from altitudes below

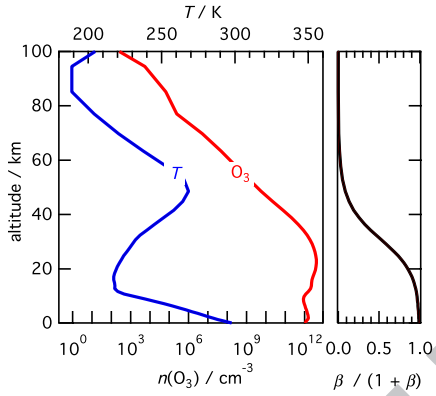


Figure 2: Typical ozone and temperature profiles of measurements in 2013 (left panel). Right panel shows $\beta/(1+\beta)$, which is an indicator for the contribution of the pressure broadened halfwidth to the overall line width.

34 km. The Voigt shape parameter

$$\beta = \gamma_L/\gamma_G \tag{4}$$

where $\gamma_L$ and $\gamma_G$ are Lorentzian and Gaussian halfwidths, respectively, can be used to quantify the importance of pressure broadening on the line shape. The function $\beta/(1+\beta)$, in particular, is a measure for the contribution of pressure broadening to the total linewidth. It takes a value of 39 % at 34 km, and increases steadily with decreasing altitude, indicating that pressure broadening is dominating in the altitude range somewhat below 34 km.

### *3.2. Sensitivity study at 10 μm*

In order to identify spectroscopic requirements and understand differences between spectroscopic databases, we have determined the sensitivity of the ozone column $C_{O_3}$ to the intensity ($S$), air-broadened half width ($\gamma_{air}$), its temperature coefficient ($n_{air}$) and the lower state energy ($E''$) expressed as equivalent wavenumber.

Line shape parameters beyond the Voigt profile due to Dicke narrowing, speed effects (velocity changing collisions and speed dependence of pressure broadening and shifting) and due to line-mixing are not yet routinely provided by the databases. We

therefore don't discuss these effects here. Actually, non-Voigt effects on isolated ozone lines can be safely neglected, since their impact on the total ozone column is 0.1 % or less [51]. However, neglecting line-mixing effects can bias the ozone total column retrieval in the 10 µm range by up to 2 % [52], but in section 4 we will present evidence that if any, the impact of line-mixing on total ozone column values in our study is likely significantly smaller (< 1 %).

We here define the sensitivity coefficient $\alpha$ as the proportionality factor between relative changes of $C_{O_3}$ due to relative changes of the respective parameter $x \in (S, \gamma_{air}, n_{air}, E'')$, i.e.:

$$\frac{\Delta C_{O_3}}{C_{O_3}} = \alpha(x) \frac{\Delta x}{x} . \tag{5}$$

Related definitions, such as the band specific sensitivity $\alpha_I(x)$ and corresponding weight factors $w_I$ are given in Appendix A.1.

Table 4 gives intensity weights $w_I$ in the 10 µm window for the bands that account for more than 99 % of the absorbed intensity at $T = 235$ K. It indicates that the fundamentals {001,100} ← 000 should contribute about 93 % to the retrieved signal. The second most important transition is the hot band from the $\nu_2 = 1$ lower state (∼5 %).

Note that calculated weights are only approximate. In the atmosphere, radiation transfer based on the Beer-Lambert law

$$I(\nu) = I_0(\nu) \exp\left( - \int n_{O_3}(z) \sum_l S_l(z)\, g_l(\nu, z)\, dz \right) \tag{6}$$

(here given for a single absorber with multiple absorption lines $l$ of line shape $g_l(\nu, z)$ and a vertical number density profile $n_{O_3}(z)$ and neglecting the apparatus function) will introduce a non-linearity, because the exponential preferentially damps stronger transitions. On the contrary, the averaging in eqs. (A.3) and (A.2) which is used to determine the contribution of individual bands to the overall signal in Table 4, does not take this dampening into account and must therefore overestimate strong absorption lines.

*3.2.1. Sensitivity on line intensity*

The optical density is defined as the negative of the exponent in the Beer-Lambert law (eq. (6)):

$$\tau(\nu) = \ln\left(\frac{I_0(\nu)}{I(\nu)}\right) = \int n_{O_3}(z) \sum_l S_l(z)\, g_l(\nu, z)\, dz. \quad (7)$$

$\tau$ is thus linear in both, $S$ and $n_{O_3}$. Since the total ozone column (eq. (2)) is also linear in $n_{O_3}$, but independent of $S$, the line intensity and $C_{O_3}$ are directly anti-correlated and $\alpha(S) = -1$. This value (−0.98) is indeed obtained for the sum of all bands (see Table 4). For individual bands, however, some deviation from the average is observed and values between 0.8 and 1.8 times of the average are obtained. As discussed before, the non-linearity of eq. (6) and the simplifying assumption of an isothermal atmosphere contribute to this difference. The $\nu_3$ fundamental, in particular, shows a sensitivity $|\alpha(S)| < 1$, which is in line with the expectation that the band with the strongest transitions should have a sensitivity weaker than average. Evidently, there must be other bands that compensate for this deficit, explaining the relatively large value for the hot band from the $\nu_2 = 1$ lower state.

For the discussion of the sensitivity to other parameters ($\gamma_{air}$, $n_{air}$), ratios of $\alpha$-values are also presented in Table 4.

*3.2.2. Sensitivity on pressure broadening coefficient*

Inspection of Table 4 reveals that $|\alpha(\gamma_{air})|$ is roughly three to six times smaller than $|\alpha(S)|$. Intensity corrected values $|\alpha(\gamma_{air})/\alpha(S)|$ are between 0.15 and 0.3. However, a striking feature in Table 4 is the opposite sign of $\alpha(\gamma_{air})$ for $001 \leftarrow 000$ as compared to the other vibrational bands. As shown in a simple numerical simulation in Appendix A.2, this is caused by line shape biases which are different for high and low peak center optical densities $\tau_0$, which must affect the strong $001 \leftarrow 000$ band differently than the others.

An empirical correlation between line intensity and peak center optical density $\tau_0$ has been derived from the atmospheric spectra (Fig. 1) using some lines around 992 and 1006 $cm^{-1}$. By comparison with the characteristic intensity of each band (obtained as intensity weighted average, see supplementary material), $\tau_0 \simeq 9$ and $\alpha(\gamma_{air}) < 0$ is

estimated for the 001←000 fundamental, whereas the range $0.08 \leq \tau_0 \leq 0.6$ corresponding to $\alpha(\gamma_{air}) \simeq +0.4$ is derived for the remaining weak bands (see Fig. A.7e).

Due to the simplifying approach of characterizing the bands by their weighted intensity and due to using an empirical correlation and ignoring the vertical atmospheric structure, it is not surprising that the agreement between the simple modeling and our observations is only semi-quantitative and that the sensitivity for the $\nu_3$ fundamental is overestimated by our approach. Nevertheless, the sign change with intensity as well as the sensitivity coefficient $|\alpha(\gamma_{air})/\alpha(S)| \simeq 0.3$ in Table 4 for the weak band transitions is quite well reproduced by the simple estimation. The modeling results thus confirm our interpretation of the sensitivity coefficient being a fitting artefact due to biases in $\gamma_{air}$.

*3.2.3. Sensitivity on temperature coefficient of pressure broadening*

The temperature coefficient $n_{air}$ determines the temperature dependence of the pressure broadening coefficient

$$\gamma_{air}(T) = \gamma_{air}(296\,\mathrm{K}) \left( \frac{296\,\mathrm{K}}{T} \right)^{n_{air}} . \tag{8}$$

Biases in $n_{air}$ are therefore directly linked to biases in $\gamma_{air}$, especially if measurements or observations are made at one particular temperature. We therefore expect that there is a strong correlation between the sensitivity coefficients of these two parameters. The ratio $\alpha(\gamma_{air})/\alpha(n_{air})$ for an isothermal atmosphere might be derived from the above eq. (8) by taking the derivative of $\gamma_{air}$ with respect to $n_{air}$ and keeping the lowest order correction (note that we drop the index *air* for the moment)

$$\begin{aligned} \frac{\Delta\gamma}{\gamma}(T) &= \left( \frac{296\,\mathrm{K}}{T} \right)^{\Delta n} - 1 \\ &\simeq n \ln\left( \frac{296\,\mathrm{K}}{T} \right) \frac{\Delta n}{n}. \end{aligned} \tag{9}$$

which directly leads to

$$\frac{\alpha(\gamma)}{\alpha(n)} \simeq n^{-1} \ln^{-1}\left( \frac{296\,\mathrm{K}}{T} \right). \tag{10}$$

For the two 011 ← 010 and 002 ← 001 hot bands and the $\nu_1$ fundamental, the databases give ranges between 0.72 and 0.80 (H12) or 0.73 and 0.76 (G11) for the

intensity weighted temperature coefficients $n_{air}$ (see supplementary material). Using our characteristic ozone temperature from eq. (3) of 235 K and following eq. (10), these values correspond to sensitivity ratios $\alpha(\gamma_{air})/\alpha(n_{air})$ between 5.4 and 6.1 (H12) and between 5.7 and 5.9 (G11). These ranges are very consistent with the observed range from 5.3 to 5.6 defined by the two strongest of the weak transitions in Table 4. Given the large measurement uncertainties, especially for the weak bands that contribute by only about 1 % to the overall absorption signal, this agreement might be somewhat accidental, as indicated by the value of 4.3 for the $\nu_3$ hot band, which is somewhat below the expected range.

#### *3.2.4. Sensitivity on lower state energy*

The main impact of the lower state energy $E''$ (or its equivalent wavenumber value) on the intensity, and thus on the ozone column, is via the Boltzmann factor $F_B(T)$ in eq. (1) [see 35, for example]. It is thus evident that

$$\frac{\Delta C_{O_3}}{C_{O_3}} = -\frac{\Delta S}{S} = \frac{c_2}{T}\Delta E''. \tag{11}$$

At 235 K, $c_2/T = 6.1 \cdot 10^{-3}$ cm and due to lower state energies being usually known better than $10^{-2}$ cm$^{-1}$, the uncertainties in $E''$ have a negligible ($< 10^{-4}$) impact on the (relative) uncertainty of the column measurements.

## 4. Database comparison

### *4.1. 10 µm region*

Fig. 3 shows retrieval results for total ozone column densities from the 10 µm region at Paris during six summer days around noon using the G11, H12 and S15 databases. The left panel demonstrates that column density retrievals give similar values when either of the three databases is used. Within one four-hour observation period, ozone columns are between 8.3 and $9.7 \cdot 10^{18}$ cm$^{-2}$ and vary only on the 1 % scale ($\sim 0.1 \cdot 10^{18}$ cm$^{-2}$). However the data reveal a small systematic bias between the three databases. Columns retrieved using the H12 database are always higher than columns from S15 and G11, and retrievals using G11 always give the lowest results. Indeed,

the right panel of Fig. 3 well illustrates that the respective offsets of −0.604 % and −0.288 % between the G11 and H12 and the S15 and H12 databases are quite significant. The scatter ($\sigma$ = 0.008 %, $N$ = 95 for G11 and $\sigma$ = 0.028 %, $N$ = 95 for S15) is comparatively small.

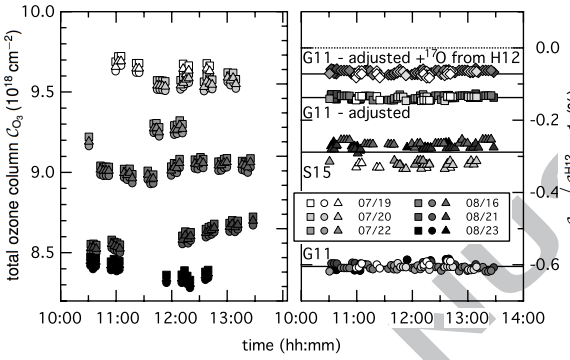


Figure 3: Total ozone column densities $C_{O_3}$ around noon during six measurement days in summer 2013 from retrievals in the 10 µm window (10−1). Left panel shows absolute values retrieved with H12 (squares), G11 (circles) and S15 (triangles) spectroscopic data. Right panel gives the relative deviation of retrieval results in percent. Circles and triangles correspond to results with unmodified G11 and S15 spectroscopic data, respectively. Squares are differences when bandwise corrections are applied to $^{16}$O and $^{18}$O-containing ozone in G11. Diamonds indicate deviations when $^{17}$O data from H12 are added to the modified G11 data.

Most of the bias between G11 and H12 is due to systematic differences in the average spectral parameters. Table 5 demonstrates that some intensity weighted spectral parameters, and even intensity values, differ by several percent. If $S$, $\gamma_{\mathrm{air}}$ and $n_{\mathrm{air}}$ in G11 are thus adjusted bandwise by the ratio $x_{\mathrm{H12}}/x_{\mathrm{G11}}$ to compensate for these differences, the relative bias is reduced to a value of only −0.138 % ($\sigma$ = 0.005 %, $N$ = 95), as shown in the right panel of Fig. 3. Interestingly, correcting for systematic biases between H12 and S15 using the same method does not improve the relative deviation in the column values; at the same time the dispersion of the data is significantly reduced. The results are not shown in Fig. 3, but we get a −0.323 % offset with a $\sigma$ = 0.007 % dispersion when we apply the standard correction procedure based on the weighted averages in Table 5. The reduction of the dispersion is mainly due to the difference in $\gamma_{\mathrm{air}}$. As a matter of fact, correcting for differences in the weighted averages of $\gamma_{\mathrm{air}}$ alone results in an offset of −0.332 % with a 0.006 % scatter. This is quite similar to

using the actual values of $\gamma_{\mathrm{air}}$ in H12 with intensities of S15. In this case the offset is $-0.227\,\%$ with a standard deviation of $\sigma = 0.007\,\%$. The comparison using the three databases also shows that using $\gamma_{air}$ from either H12 or G11 leads to a small dispersion in the retrieved columns, whereas the dispersion is about four times higher when S15 is compared to H12. Note, that relative differences in weighted $\gamma_{air}$ are also four times higher when we compare the $\nu_3$ transition of the main isotope in S15 and G11 with respect to the corresponding values in H12 (see Table 5).

As can also be inferred from the sensitivity coefficients in Table 4, a global correction of about 0.21 %, 1.15 % and 1.10 % applied to the respective values of $S$, $\gamma_{air}$ and $n_{\mathrm{air}}$ in G11, irrespective of the vibrational band, would only account for a small fraction of the observed total column difference and it is essential to consider vibrational states individually. The need for bandwise correction is thus evident and this is also clear from direct inspection of Table 5, which shows strong differences between the databases concerning hot band transitions: hot band intensities of $^{16}O_3$ in H12 are 1.6 and 4 % lower than in G11, for example. This, and the fact that fundamentals of the $^{18}$O containing isotopomers also deviate by about 4 % between the two databases, possibly indicates that intensities of the hot bands were globally changed in the 2000 to 2004 update of H12, whereas most of the G11 data remained unchanged. Depending on isotopes or transitions, differences in $\gamma_{\mathrm{air}}$ can also be quite sizable and reach values of up to 13 % (Table 5). Some of the remaining discrepancy between ozone columns derived from G11 and H12 spectral parameters is due to the complete lack of $^{17}$O containing ozone in the 10 µm region in G11. If also taken into account, the bias between databases drops well below 1 ‰ (see right panel of Fig. 3). Interestingly, this good agreement between the atmospheric radiation transfer modeling and the global bandwise analysis can only be obtained in the comparison between G11 and H12 databases. Applying the same correction procedures to the S15 data does not remove the $-3$ ‰ offset between the column values from H12 and S15. The reasons for this difference are detailed just below.

The lower right panel of Fig. 4, which compares H12 with G11, shows that most of the intense bands in the 10 µm region differ by a constant value (either 0 or 4 %). Only the $011 \leftarrow 010$ hot band, which contributes about 5 % to the overall absorption

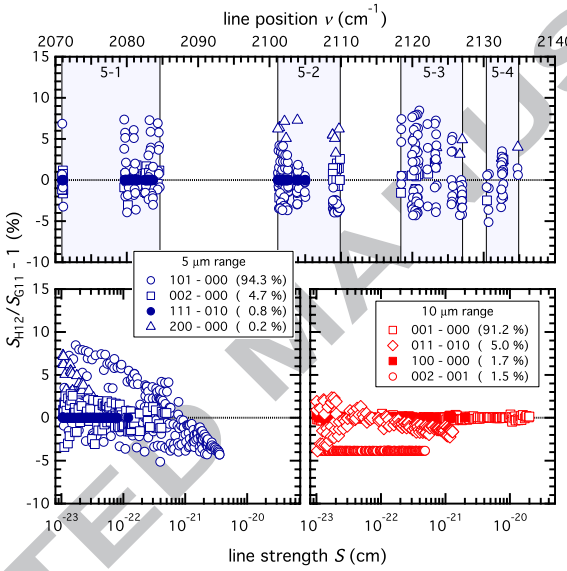


Figure 4: Relative deviation of intensities of individual $^{16}O_3$ transitions between H12 and G11 databases as a function of line position (top) and of intensity $S(296\,\mathrm{K}) \geq 10^{-23}$ cm (bottom). Top: individual windows (5−1 to 5−4) in the 5 µm range are indicated by shadows. Bottom: Left panel 5 µm, right panel 10 µm data. Line data common to the two databases and corresponding to the four most intense bands (with weights given in the legends) are shown.

shows some scatter and a slight negative correlation in this wavelength region. The presence of such a correlation introduces a bias in the database comparison based on intensity weighted averages (see Appendix B, for example). These correlations are stronger when we compare H12 to S15. The lower right panel of Fig. 5 shows that a positive correlation even exists in the most intense transitions of the $\nu_3$ band. From

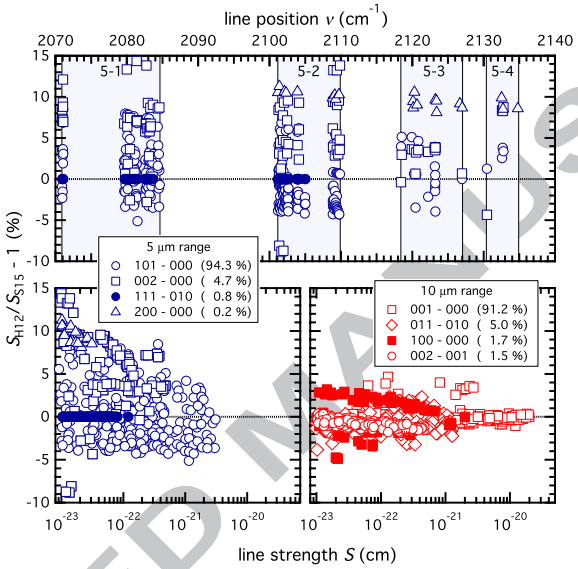


Figure 5: Relative deviation of intensities of individual $^{16}O_3$ transitions between H12 and S15 databases as a function of line position (top) and of intensity $S(296\,\mathrm{K}) \geq 10^{-23}$ cm (bottom). Top: individual windows (5−1 to 5−4) in the 5 µm range are indicated by shadows. Bottom: Left panel 5 µm, right panel 10 µm data. Line data common to the two databases and corresponding to the four most intense bands (with weights given in the legends) are shown.

a linear fit of $\Delta S/S$ vs. $S(235\,K)$ in the range $S > 10^{-21}$ cm on transitions in the $\nu_3$ band of the main isotope, we derive a slope of $+3.6 \cdot 10^{17}\,\mathrm{cm}^{-1}$ and inspection of the H12 database shows that $2[E(S^3)/E(S^2) - E(S^2)/E(S)] = 7.9 \cdot 10^{-21}$ cm (for further details see Appendix B). According to eq. (B.6), this results in an overrestimation of the adjusted intensities by about 0.3 %. Ozone columns will thus be underestimated by the same relative amount, when adjusted intensity values are used and this corresponds exactly to the observed difference between retrievals based on S15 and H12 displayed in Fig. 3.

### 4.2. 5 μm region

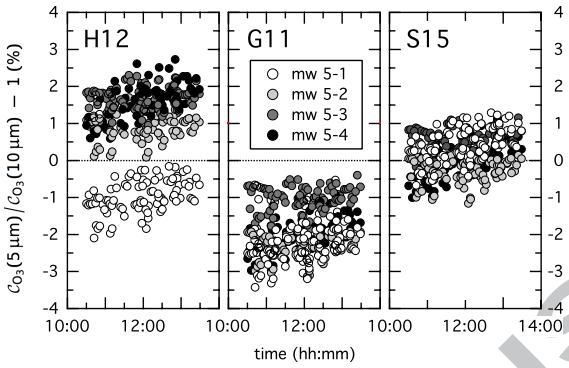


Figure 6: Total ozone column densities $C_{O_3}$ from the 5 μm windows 5−1 to 5−4 as relative deviation with respect to the retrieval from the 10 μm window (10−1). Panels from left to right show results for the H12, G11 and S15 database, respectively. Individual 5 μm windows are indicated by symbol shades.

Column densities from the 5 μm windows are represented in Fig. 6 as relative deviation from the result in the 10 μm window. Independent of the database, the results from the two wavelength regions are coherent to better than ±3 %. Averages over individual windows are within −1.0 and +1.6 % for H12, within −1.0 and −2.3 % for G11 and within −0.3 and +0.5 % for S15. While G11 data thus give a consistent negative offset of about (−1.9 ± 0.6) % (1 $\sigma$ dispersion of window averages) with little dispersion and while S15 has an insignificant offset with an even smaller dispersion of (0.2 ± 0.4) %, the H12 data have a positive offset of (1.4 ± 0.4) % for windows 5−2 through 5−4. The 5−1 window, which is dominated by transitions belonging to the *P*-branch of the $\nu_1 + \nu_3$ band, however is not consistent with this positive shift and shows an offset of −1.0 %. Note that the dispersion within each window (1 $\sigma$, $N = 93$) is in the 0.3 to 0.4 % range. This single intra-window dispersion is independent of the window and the database used and thus mereley reflects measurement uncertainties.

We point out that our atmospherically observed offset of +1.4 % between 5 and 10 μm regions when using H12 is in full agreement with a recent laboratory study [27]. The laboratory derived intensities deviate from H12 by (−1.96 ± 0.29) and (−0.34±0.11) % at 5 and 10 μm, respectively. This implies $C^{H12}_{O_3}(5\,\mu m)/C^{H12}_{O_3}(10\,\mu m) =$ (+1.6 ± 0.3) %, where the 1-$\sigma$ uncertainty is derived from the propagation of the sta-

tistically derived uncertainty of the individual averages at 5 and 10 μm. The comparison with this measurement and the fact that line-mixing does not measurably change total ozone columns from the 5 μm range under atmospheric conditions [52, see Table 1], let us conclude that line-mixing impacts total ozone columns from the 10 μm region (window 10−1) by an amount less than the dispersion of our measurements. A similar conclusion must be drawn from the comparison with the slightly higher value $C^{\mathrm{H12}}_{\mathrm{O_3}}(5\,\mu\mathrm{m})/C^{\mathrm{H12}}_{\mathrm{O_3}}(10\,\mu\mathrm{m}) = (+2.1 \pm 0.3)\,\%$ derived in another laboratory study under high pressure conditions (0.3 − 1 bar), where line-mixing effects have been taken into account in the analysis [52]. This high degree of agreement with both laboratory experiments implies that the effect of line-mixing on the derived total ozone column densities is small and likely less than about 0.7 %. The full agreement between retrieval results from all windows within the scatter of about 0.4 % when S15 is used (right panel of Fig. 6) indeed provides very strong support for line-mixing effects actually being smaller than 0.4 %. Anyway, they are smaller than most of the effects that we are about to discuss in the following.

The differences of about 3.5 % (windows 5−2 through 5−4) between the G11 and H12 databases can be easily understood on the background of our previous analysis and discussion concerning the 10 μm region. Calculation of intensity weighted spectral parameters at 235 K shows that in each of the windows most of the absorbed intensity is due to the 101 ← 000 band. This band has a roughly 3 (5−1) to 4 % (5−2 to 5−4) higher weighted intensity in G11 than in H12 (see Table 6), implying that the column densities must be correspondingly lower. From this ∼ 4 % correction, the 0.6 % difference in the 10 μm region must be subtracted. The resulting shift in $C_{\mathrm{O_3}}(5\,\mu\mathrm{m})/C_{\mathrm{O_3}}(10\,\mu\mathrm{m})$ of 3.4 % is fully consistent with the atmospheric observation in Fig. 6. We note that intensities of these overtone and combination bands are sufficiently weak for non-linear absorption effects, such as observed in the $\nu_3$ fundamental at 10 μm, being of little importance.

Table 6 further shows that the ratio of ozone columns derived from the two databases at 5 μm $C^{\mathrm{H12}}_{\mathrm{O_3}}(5\,\mu\mathrm{m})/C^{\mathrm{G11}}_{\mathrm{O_3}}(5\,\mu\mathrm{m})$ cannot be consistent over all windows at the accuracy level of 1 %. The weighted average analysis confirms that the column ratio $C^{\mathrm{H12}}_{\mathrm{O_3}}(5\,\mu\mathrm{m})\Big/ C^{\mathrm{G11}}_{\mathrm{O_3}}(5\,\mu\mathrm{m})$ is lower in the 5−1 window than in the others. Because results from the

G11 database are consistent over all four windows, we suspect that the problem is linked to the spectroscopic data in H12. However, the simplified database comparison in Table 6 gives a difference of only 1.4 % and rests below the observed discrepancy of about 2 to 2.5 %. These database differences are further corroborated by the excellent agreement found in the S15 based retrievals.

As an aside we note here that the $111 \leftarrow 010$ hot band has identical intensity entries in all three different databases. This becomes evident from Fig. 5, but is also reflected in the corresponding entries in Table 6, which are all identical zero.

The large intensity dependent differences in line strengths of $2\nu_1$, $2\nu_3$ and $\nu_1 + \nu_3$ band transitions between the G11 and H12 databases (see left panel of Fig. 4) prevent intensity weighted averages to be used for globally rescaling one database with respect to the other in order to resolve observed discrepancies in the 5 µm region. The column biases associated with a weighted intensity correction, that are obtained from the procedure described in section 4.1 are around 1.4 %. It thus seems that this particular spectral region requires new experimental and theoretical studies to be undertaken. The high consistency of the S15 based retrievals possibly indicates that the S&MPO (S15) database presently is the most adequate to use for retrieving ozone from the 5 and 10 µm regions, and that the underlying data and spectroscopic analysis already provide the desired level of accuracy of better than 1 %. But so far these data have not been published in the literature. It must also be kept in mind that our study cannot assess the absolute accuracy of the spectroscopic data and since our observations are based on lines from very restricted spectral ranges (see Fig. 1), little can be said about data quality concerning transitions outside the observational windows.

## 5. Conclusion and Outlook

We have compared ozone spectroscopic data in the 5 and 10 µm spectral regions from different databases and confronted them with ground based atmospheric spectra, acquired with the high-resolution FTS-Paris instrument. In order to clearly attribute differences in retrieved ozone columns to differences in the spectroscopic databases, we have also performed direct database comparisons restricted to the observational

windows, using intensity weighted averages of the chief spectroscopic parameters.

Using the atmospheric spectra, a complete sensitivity analysis of the four spectroscopic parameters intensity ($S$), air-broadening half width ($\gamma_{air}$), its temperature coefficient ($n_{air}$) and the lower state energy ($E''$) has been performed in the 10 μm region. Relative uncertainties of these parameters belonging to transitions in the $\nu_3$ fundamental band impact on the total ozone columns with respective of weights $-1 : -0.15 : -0.05$ , for $S$, $\gamma_{air}$ and $n_{air}$. For transitions belonging to weaker bands in the same region, sensitivity coefficients for $S$, $\gamma_{air}$ and $n_{air}$ scale as $-1 : +0.29 : +0.055$. The observed sensitivity coefficients have been confirmed by theoretical analysis and numerical simulations. Current database uncertainties in $E''$ do not affect retrievals and can be neglected. The derived sensitivity coefficients might guide further studies that aim at improving on the uncertainty of total ozone column retrievals in that region.

The three databases HITRAN, GEISA and S&MPO have been characterized with respect to their utility for atmospheric retrievals. Using the spectroscopic data in the $991.25 - 1013.19\,\mathrm{cm}^{-1}$ window range, total ozone column retrievals with the three databases gave results that agreed to clearly better than 1 %. Much of the difference is due to slight differences in the spectroscopic data and, in case of in the GEISA database, the lack of $^{17}$O-containing ozone. This degree of agreement is confirmed by direct comparison of spectroscopic databases, using intensity weighted averages of the spectroscopic parameters.

Deviations between the databases in the 5 μm region are larger, however. Ozone columns derived in that wavelength range differ by about 4 %, which is likely due to a global adjustment of line intensities [18] in the HITRAN database in 2004, which has only partially been adopted in the GEISA database. Nevertheless, each of the three databases gives total ozone columns at 5 μm that generally agree within ±2 % with the results obtained at 10 μm. Retrievals using the S&MPO data show an even better agreement within less than ±1 %, both between the 5 and 10 μm regions and within the 5 μm region itself.

Importantly, all four windows in the 5 μm region yield consistent ozone columns when we use parameters from the GEISA or S&MPO databases. This is not the case when parameters are taken from HITRAN. Employing HITRAN parameters, one of

the windows (2070.90 − 2084.64 $cm^{-1}$), mostly containing *P*-branch transitions from the $\nu_1 + \nu_3$ combination band in the 5 μm region results in ozone columns that are significantly lower (1.5 − 3.0 %) than the ones obtained from the other three windows. This striking difference between databases is corroborated by direct comparison of the intensity weighted average intensities in the four windows. While average intensities between HITRAN and GEISA databases differ by 4.1 % in the three coherent windows, they differ by only 2.7 % in the particular window between 2070.90 and 2084.64 $cm^{-1}$. The inferred difference of 1.4 % is close to the observed discrepancy, which thus confirms that the observed mismatch is due to the ozone spectroscopic data in the two databases and not linked to the measurement process or the retrieval procedure. This fact is further corroborated by the excellent consistency of results when either GEISA or S&MPO are used for the retrieval.

While the comparison in the 10 μm region has shown that all databases yield very consistent results at a high level of precision (< 1 %), the detailed analysis of the 5 μm region shows that a similar precision level has not yet been reached there. Only the S&MPO database gives entirely consistent results at the 1 % level. Thus, further laboratory studies targetting at the 5 μm and other spectral regions are required. So are new theoretical calculations [10] and validation procedures for incorporating new line parameter data into the databases.

With the availability of more and more spectroscopic databases or linelists, the simple method of comparing intensity weighted spectroscopic parameter averages may provide an interesting tool for analyzing these databases for consistency and thus for identifying critical regions for remote sensing applications. While the approach avoids entering into the tedious work of analyzing individual transitions, it remains to be shown that its application is useful for the remote sensing of molecules other than ozone.

## Appendix A. Sensitivity

### *Appendix A.1. Band specific sensitivity coefficients and intensity weights*

In this appendix, definitions for the band specific sensitivity coefficients and intensity weights are given. We first define the band specific sensitivity coefficient $\alpha_I(x)$

$$\alpha_I(x) = \frac{1}{w_I} \left( \frac{\Delta C_{O_3}}{C_{O_3}} \right) \Big/ \left( \frac{\Delta x_I}{x_I} \right) \tag{A.1}$$

where $x_I$ indicates that parameter changes of a rovibrational transition are considered only if this transition belongs to the particular band $I$. The weight $w_I$ of the vibrational band $I$ is the defined as the ratio of the pseudo band intensity $\hat{S}_I$ over the integrated intensity of all rovibrational transitions within the considered window $M$:

$$w_I = \hat{S}_I \Big/ \sum_{j \in M} S_j, \tag{A.2}$$

where the $S_j$ are line strengths of individual rovibrational transitions $j$. The pseudo band intensity $\hat{S}_I$ corresponds to the total band intensity restricted to transitions within the observational window $M$, *i.e.*:

$$\hat{S}_I = \sum_{j \in I \,\wedge\, j \in M} S_j. \tag{A.3}$$

### *Appendix A.2. Simulation of pressure braodening*

We assume a Voigt line shape for a molecular transition and simulate molecular absorption in a homogeneous atmosphere. Three parameters are required: the Gaussian (Doppler) width which is described by the HWHM parameter $\gamma_G$, the Lorentzian width for the pressure broadening, given by the HWHM parameter $\gamma_L = \gamma_{air} \times p$, and the optical density at peak center $\tau_0$. In the atmospheric retrieval, widths are determined by temperature and pressure conditions and the corresponding values therefore are fixed in the fitting process. Nevertheless, the Lorentzian width may be off by a bias in $\gamma_{air}$. This effect is investigated through fitting a Voigt line profile with a small bias in $\gamma_L$ (1.02 times the width of the original profile), leading to a non-zero residual and a biased value for the peak area. The results of these simulations are shown in Figures A.7a-c, where transmission curves of the absorption lines and the fit residuals are displayed

for different optical densities $\tau_0$. As can be seen, the residuals change from a V to a W-shape when increasing $\tau_0$ from 0.1 to 10. For the simulation, the Doppler width has been fixed to a typical value of $\gamma_G = 0.1\,\mathrm{cm}^{-1}$, but the result is completely independent of the exact value used. It only depends on the shape parameter $\beta$ (eq. (4)), which was fixed to $\beta = 7$ in Figs. A.7 a-c for matching typical atmospheric conditions.

In Figure A.7 d, a simulated value of $\alpha(\gamma_{air})$ has been calculated by equation (5), using $\Delta x/x = 0.02$ for various combinations of $\tau_0$ and $\beta$. In the high pressure limit ($\beta \geq 10$), $\alpha(\gamma_{air})$ becomes independent of the shape parameter. This is expected, because the width is dominated by pressure broadening anyway and a bias in this parameter should have its maximum effect. In the low pressure limit ($\beta \leq 0.1$), one expects that biases in $\gamma_L$ can be neglected, because the line shape is dominated by Doppler broadening. For weak absorptions $\tau_0 < 1$, $\alpha(\gamma_{air})$ is indeed about 0. At large optical densities however, $\alpha(\gamma_{air})$ never vanishes because the wings of the Lorentzian have still an impact on the fit far from the line center, even though the HWHM width is completely dominated by the Doppler profile. This wing effect scales linearly with $\tau_0$ and the asymptotical behavior of $\alpha(\gamma_{air})$ is given by the product $\tau_0 \times \beta = const$. Figures A.7e-g then illustrate for fixed values of $\beta$ how $\alpha(\gamma_{air})$ varies as a function of the optical density. At high pressures ($\beta = 7$), it changes from about +0.45 to −1 at $\tau_0 \sim 100$ (Fig. A.7e). At low pressures, the low optical density limit approaches zero and the transition towards negative values shifts towards higher peak absorption values.

These results on $\alpha(\gamma_{air})$ are robust and do only weakly depend on the exact knowledge of $\gamma_{air}$: Comparing the fit results of two line profiles biased by 12 and 10 % in $\gamma_{air}$, respectively, gave a similar difference in retrieved intensities than comparing a line with 2 % bias to the unbiased line. Grey curves in Figures A.7e-g show the results derived from biases offset by ±10 %, which is deemed a reasonable range for the uncertainty of the published data. Because it is independent on pressure in the $\beta \geq 7$ range which is characteristic for most of the vertical ozone distribution (see section 3.1), $\alpha(\gamma_{air})$ should follow the $\tau_0$ dependency given in Figure A.7e.

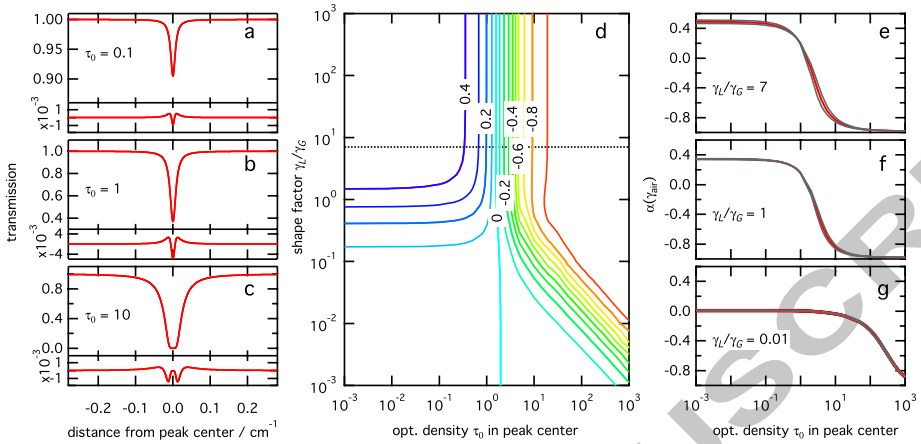


Figure A.7: Sensitivity of the column on biases in the $\gamma_{air}$ parameter from a simple numerical simulation. Panels a through c show Voigt profiles and fit residuals, when $\gamma_{air}$ is biased by +2% for peak center optical densities $\tau_0$ of 0.1, 1, and 10, respectively. The Gaussian HWHM, and the shape parameter have respectively been fixed to characteristic value of $\gamma_G = 0.1\,\mathrm{cm}^{-1}$ and $\beta = \gamma_L/\gamma_G = 7$. Panel d shows $\alpha(\gamma_{air})$ as a function of the peak absorption $\tau_0$ and the shape parameter $\gamma_L/\gamma_G$. Contour lines are separated by units of 0.1 and the dashed horizontal line indicates $\beta = 7$. Panels e to g then display $\alpha(\gamma_{air})$ as a function of the peak optical density $\tau_0$ for $\beta$ fixed to values of 7, 1, and 0.01 (red lines). Grey lines indicate in as much the bias of $\alpha(\gamma_{air})$ depends on the absolute value $\gamma_{air}$. Shaded regions in panels e-g indicate estimated atmospheric absorption conditions for the asymmetric stretch ($\nu_3$) with $\tau_0 \simeq 9$ on the one hand and the weaker bands ($0.08 \leq \tau_0 \leq 0.6$) on the other hand.

## Appendix B. Bias of intensity weighted averages

We have introduced intensity weighted averages as a practical means of direct comparison of spectroscopic parameters in different databases, which introduces an effective cutoff of weak absorption lines. Here we show that correcting values in one database by the ratio of averages between the two databases does not necessarily reproduce the results of the latter in an atmospheric retrieval and thus introduces a bias. This depends on whether the spectroscopic data correlate with the line intensities or not.

We start from the idealizing assumption that each line contributes to the retrieved absorption signal proportional to its line intensity (*ie* we neglect the presence of noise in the atmospheric measurement). The expectation value or mean $E$ of the statistic of

intensities $S$ is defined by

$$E(S) = \frac{1}{N}\sum_{i=1}^{N} S_i. \tag{B.1}$$

For what follows, we recall that the second and third moments of $S$ are similarly defined as $E(S^2)$ and $E(S^3)$, respectively. Like $E(S)$, these quantities can be easily calculated from the data given in the spectroscopic databases. We assume that the values in the two databases $S_{\mathrm{H}}$ and $S_{\mathrm{G}}$ suffer from small biases with respect to the true distribution of intensity values $S$ :

$$S_{\mathrm{H}} = (1 + a + bS)S \tag{B.2}$$

$$S_{\mathrm{G}} = (1 + c + dS)S \tag{B.3}$$

The coefficients $a$ and $c$ denote relative offsets of the database values with respect to the true values and coefficients $b$ and $d \neq 0$ indicate a linear correlation of the bias with intensity. In this case the ratio $R$ of expectation values is given by

$$\begin{aligned} R &= \frac{E(S_{\mathrm{H}})}{E(S_{\mathrm{G}})} = \frac{E\left((1 + a + bS)S\right)}{E\left((1 + c + dS)S\right)} \\ &\simeq \frac{1+a}{1+c}\left(1 + (b-d)\frac{E\left(S^2\right)}{E\left(S\right)}\right), \end{aligned} \tag{B.4}$$

where the last transformation holds to the degree that terms of second order in the supposedly small deviations $a$, $b$, $c$ and $d$ can be neglected. Due to the ratio of weighted averages $E_w$ (eqs. (A.3) and (A.2)) being

$$R_w = \frac{E_w(S_{\mathrm{H}})}{E_w(S_{\mathrm{G}})} = R^{-1}\frac{E(S_{\mathrm{H}}^2)}{E(S_{\mathrm{G}}^2)}, \tag{B.5}$$

we find that

$$\begin{aligned} R_w/R &= R^{-2}\frac{E(S_{\mathrm{H}}^2)}{E(S_{\mathrm{G}}^2)} \\ &\simeq 1 + 2(b-d)\left(\frac{E(S^3)}{E(S^2)} - \frac{E(S^2)}{E(S)}\right), \end{aligned} \tag{B.6}$$

where in the last step we have once again neglected higher than linear order terms in $a$, $b$, $c$ and $d$. Our bias is thus given by the second term in equation (B.6). Evidently, only if $b \neq d$, we introduce a bias by comparing intensity weighted averages. Note that if

$b = d = 0$, the approximations in eqs. (B.4) and (B.6) become exact and any constant relative offset between the two databases is inferred without any bias.

A non-zero term $(b - d)$ might be inferred as the slope of the linear fit on the $\Delta S/S$ over $S$ data, such as in Fig. 4 and the expression in parantheses can be simply estimated from using either $S_{\mathrm{H}}$ or $S_{\mathrm{G}}$ for the unknown $S$. In this way the bias can be determined and accounted for.

**Acknowledgement**

This work was supported by the french national programme LEFE/INSU. The authors would like to express their gratitude for the valuable technical support of H. Elandaloussi, P. Marie-Jeanne, and C. Rouillé.

**References**

[1] J. Viallon, P. Moussay, J. E. Norris, F. R. Guenther, R. I. Wielgosz, Metrologia 43 (2006) 441–450.

[2] P. J. Nair, S. Godin-Beekmann, J. Kuttippurath, G. Ancellet, F. Goutail, A. Pazmino, L. Froidevaux, J. M. Zawodny, R. D. Evans, H. J. Wang, Atmos. Chem. Phys. 13 (2013) 10373–10384.

[3] S. B. Andersen, E. C. Weatherhead, A. Stevermer, J. Austin, C. Brühl, E. L. Fleming, J. de Grandpré, V. Grewe, I. Isaksen, G. Pitari, J. Geophys. Res. Atmos. 111 (2006).

[4] C. Vigouroux, T. Blumenstock, M. Coffey, Q. Errera, O. García, N. B. Jones, J. W. Hannigan, F. Hase, B. Liley, E. Mahieu, J. Mellqvist, J. Notholt, M. Palm, G. Persson, M. Schneider, C. Servais, D. Smale, L. Thölix, M. De Mazière, Atmos. Chem. Phys. 15 (2015) 2915–2933.

[5] A. Tandon, A. K. Attri, Atmos. Environ. 45 (2011) 1648–1654.

[6] C. Janssen, D. Simone, M. Guinet, Rev. Sci. Instr. 82 (2011) 034102. doi:10.1063/1.3557512.

[7] M. Petersen, J. Viallon, P. Moussay, R. I. Wielgosz, J. Geophys. Res. 117 (2012).

[8] J. Viallon, S. Lee, P. Moussay, K. Tworek, M. Petersen, R. I. Wielgosz, Atmos. Meas. Tech. 8 (2015) 1245–1257.

[9] J. M. Flaud, R. Bacis, Spectrochim. Acta A 54 (1998) 3–16.

[10] A. Barbe, S. Mikhailenko, E. Starikova, M. R. De Backer, V. Tyuterev, D. Mondelain, S. Kassi, A. Campargue, C. Janssen, S. Tashkun, J. Quant. Spectrosc. Radiat. Trans. 130 (2013) 172–190.

[11] B. Hassler, I. Petropavlovskikh, J. Staehelin, T. August, P. K. Bhartia, C. Clerbaux, D. Degenstein, M. D. Mazière, B. M. Dinelli, A. Dudhia, G. Dufour, S. M. Frith, L. Froidevaux, S. Godin-Beekmann, J. Granville, N. R. P. Harris, K. Hoppel, D. Hubert, Y. Kasai, M. J. Kurylo, E. Kyrölä, J. C. Lambert, P. F. Levelt, C. T. McElroy, R. D. McPeters, R. Munro, H. Nakajima, A. Parrish, P. Raspollini, E. E. Remsberg, K. H. Rosenlof, A. Rozanov, T. Sano, Y. Sasano, M. Shiotani, H. G. J. Smit, G. Stiller, J. Tamminen, D. W. Tarasick, J. Urban, R. J. van der A, J. P. Veefkind, C. Vigouroux, T. von Clarmann, C. von Savigny, K. A. Walker, M. Weber, J. Wild, J. M. Zawodny, Atmos. Meas. Tech. 7 (2014) 1395–1427.

[12] M. A. H. Smith, V. M. Devi, D. C. Benner, C. P. Rinsland, J. Geophys. Res. 106 (2001) 9909–9921.

[13] C. Claveau, C. Camy-Peyret, A. Valentin, J. M. Flaud, J. Molec. Spectrosc. 206 (2001) 115–125.

[14] G. Wagner, M. Birk, F. Schreier, J. M. Flaud, J. Geophys. Res. 107 (2002) 4626. doi:10.1029/2001JD000818.

[15] M. R. DeBacker-Barilly, A. Barbe, J. Molec. Spectrosc. 205 (2001) 43–53.

[16] J. M. Flaud, G. Wagner, M. Birk, C. Camy-Peyret, C. Claveau, M. R. DeBacker-Barilly, A. Barbe, C. Piccolo, J. Geophys. Res. 108 (2003). doi:10.1029/2002JD002755.

[17] N. Jacquinet-Husson, N. Scott, A. Chedin, K. Garceran, R. Armante, A. Chursin, A. Barbe, M. Birk, L. Brown, C. Camy-Peyret, C. Claveau, C. Clerbaux, P. Coheur, V. Dana, L. Daumont, M. Debacker-Barilly, J. Flaud, A. Goldman, A. Hamdouni, M. Hess, D. Jacquemart, P. Kopke, J. Mandin, S. Massie, S. Mikhailenko, V. Nemtchinov, A. Nikitin, D. Newnham, A. Perrin, V. Perevalov, L. Regalia-Jarlot, A. Rublev, F. Schreier, I. Schult, K. Smith, S. Tashkun, J. Teffo, R. Toth, V. Tyuterev, J. Auwera, P. Varanasi, G. Wagner, J. Quant. Spectroscop. Radiat. Transfer 95 (2005) 429–467.

[18] L. S. Rothman, D. Jacquemart, A. Barbe, D. C. Benner, M. Birk, L. R. Brown, M. R. Carleer, C. Chackerian, Jr, K. Chance, L. H. Coudert, V. Dana, V. M. Devi, J.-M. Flaud, R. R. Gamache, A. Goldman, J.-M. Hartmann, K. W. Jucks, A. G. Maki, J.-Y. Mandin, S. T. Massie, J. Orphal, A. Perrin, C. P. Rinsland, M. A. H. Smith, J. Tennyson, R. N. Tolchenov, R. A. Toth, J. Vander Auwera, P. Varanasi, G. Wagner, J. Quant. Spectrosc. Radiat. Trans. 96 (2005) 139 – 204.

[19] L. S. Rothman, I. E. Gordon, A. Barbe, D. C. Benner, P. F. Bernath, M. Birk, V. Boudon, L. R. Brown, A. Campargue, J. P. Champion, K. Chance, L. H. Coudert, V. Dana, V. M. Devi, S. Fally, J. M. Flaud, R. R. Gamache, A. Goldman, D. Jacquemart, I. Kleiner, N. Lacome, W. J. Lafferty, J. Y. Mandin, S. T. Massie, S. N. Mikhailenko, C. E. Miller, N. Moazzen-Ahmadi, O. V. Naumenko, A. V. Nikitin, J. Orphal, V. I. Perevalov, A. Perrin, A. Predoi-Cross, C. P. Rinsland, M. Rotger, M. Simecková, M. A. H. Smith, K. Sung, S. A. Tashkun, J. Tennyson, R. A. Toth, A. C. Vandaele, J. Vander Auwera, J. Quant. Spectrosc. Radiat. Trans. 110 (2009) 533–572.

[20] A. Gratien, B. Picquet-Varrault, J. Orphal, J. F. Doussin, J. M. Flaud, J. Phys. Chem. A 114 (2010) 10045–10048. doi:10.1021/jp103992f.

[21] B. Picquet-Varrault, J. Orphal, J.-F. Doussin, P. Carlier, J.-M. Flaud, J. Phys. Chem. A 109 (2005) 1008 – 1014. doi:10.1021/jp0405411.

[22] C. Viatte, M. Schneider, A. Redondas, F. Hase, M. Eremenko, P. Chelin, J. M.

Flaud, T. Blumenstock, J. Orphal, Atmos. Meas. Tech. 4 (2011) 535–546. doi:10.5194/amt-4-535-2011.

[23] E. Dupuy, K. A. Walker, J. Kar, C. D. Boone, C. T. McElroy, P. F. Bernath, J. R. Drummond, R. Skelton, S. D. McLeod, R. C. Hughes, C. R. Nowlan, D. G. Dufour, J. Zou, F. Nichitiu, K. Strong, P. Baron, R. M. Bevilacqua, T. Blumenstock, G. E. Bodeker, T. Borsdorff, A. E. Bourassa, H. Bovensmann, I. S. Boyd, A. Bracher, C. Brogniez, J. P. Burrows, V. Catoire, S. Ceccherini, S. Chabrillat, T. Christensen, M. T. Coffey, U. Cortesi, J. Davies, C. De Clercq, D. A. Degenstein, M. De Mazière, P. Demoulin, J. Dodion, B. Firanski, H. Fischer, G. Forbes, L. Froidevaux, D. Fussen, P. Gerard, S. Godin-Beekmann, F. Goutail, J. Granville, D. Griffith, C. S. Haley, J. W. Hannigan, M. Höpfner, J. J. Jin, A. Jones, N. B. Jones, K. Jucks, A. Kagawa, Y. Kasai, T. E. Kerzenmacher, A. Kleinböhl, A. R. Klekociuk, I. Kramer, H. Küllmann, J. Kuttippurath, E. Kyrölä, J.-C. Lambert, N. J. Livesey, E. J. Llewellyn, N. D. Lloyd, E. Mahieu, G. L. Manney, B. T. Marshall, J. C. McConnell, M. P. McCormick, I. S. McDermid, M. McHugh, C. A. McLinden, J. Mellqvist, K. Mizutani, Y. Murayama, D. P. Murtagh, H. Oelhaf, A. Parrish, S. V. Petelina, C. Piccolo, J.-P. Pommereau, C. E. Randall, C. Robert, C. Roth, M. Schneider, C. Senten, T. Steck, A. Strandberg, K. B. Strawbridge, R. Sussmann, D. P. J. Swart, D. W. Tarasick, J. R. Taylor, C. Tétard, L. W. Thomason, A. M. Thompson, M. B. Tully, J. Urban, F. Vanhellemont, C. Vigouroux, T. von Clarmann, P. von der Gathen, C. von Savigny, J. W. Waters, J. C. Witte, M. Wolff, J. M. Zawodny, Atmos. Chem. Phys. 9 (2009) 287–343.

[24] L. S. Rothman, A. Barbe, D. Chris Benner, L. R. Brown, C. Camy-Peyret, M. R. Carleer, K. Chance, C. Clerbaux, V. Dana, V. M. Devi, A. Fayt, J. M. Flaud, R. R. Gamache, A. Goldman, D. Jacquemart, K. W. Jucks, W. J. Lafferty, J. Y. Mandin, S. T. Massie, V. Nemtchinov, D. A. Newnham, A. Perrin, C. P. Rinsland, J. Schroeder, K. Smith, M. A. H. Smith, K. Tang, R. A. Toth, J. Vander Auwera, P. Varanasi, K. Yoshino, J. Quant. Spectroscop. Radiat. Trans. 82 (2003) 5–44.

[25] M. Guinet, D. Mondelain, C. Janssen, C. Camy-Peyret, J. Quant. Spectrosc. Radiat. Trans. 111 (2010) 961–972.

[26] D. G. Dufour, J. R. Drummond, C. T. McElroy, C. Midwinter, P. F. Bernath, K. A. Walker, W. F. J. Evans, E. Puckrin, C. Nowlan, J. Phys. Chem. A 109 (2005) 8760–8764.

[27] X. Thomas, P. Von Der Heyden, M. R. De Backer-Barilly, M. T. Bourgeois, A. Barbe, J. Quant. Spectrosc. Radiat. Trans. 111 (2010) 1080–1088. doi:10.1016/j.jqsrt.2010.02.001.

[28] K. A. Walker, C. Boone, R. Skelton, S. D. McLeod, P. F. Bernath, C. E. Randall, C. R. Trepte, K. Strong, T. C. McElroy, in: ENVISAT Symposium April 2007, Montreux (Switzerland).

[29] O. E. García, M. Schneider, F. Hase, T. Blumenstock, E. Sepulveda, Y. González, Atmos. Meas. Tech. 7 (2014) 3071–3084.

[30] M. Schneider, F. Hase, J. Quant. Spectroscop. Radiat. Trans. 110 (2009) 1825–1839.

[31] N. Jacquinet-Husson, L. Crepeau, R. Armante, C. Boutammine, A. Chedin, N. Scott, C. Crevoisier, V. Capelle, C. Boone, N. Poulet-Crovisier, A. Barbe, A. Campargue, D. Chris Benner, Y. Benilan, B. Bézard, V. Boudon, L. R. Brown, L. H. Coudert, A. Coustenis, V. Dana, V. M. Devi, S. Fally, A. Fayt, J. M. Flaud, A. Goldman, M. Herman, G. Harris, D. Jacquemart, A. Jolly, I. Kleiner, A. Kleinböhl, F. Kwabia-Tchana, N. Lavrentieva, N. Lacome, L.-H. Xu, O. Lyulin, J. Y. Mandin, A. Maki, S. Mikhailenko, C. E. Miller, T. Mishina, N. Moazzen-Ahmadi, H. Müller, A. Nikitin, J. Orphal, V. Perevalov, A. Perrin, D. Petkie, A. Predoi-Cross, C. P. Rinsland, J. Remedios, M. Rotger, M. A. H. Smith, K. Sung, S. Tashkun, J. Tennyson, R. A. Toth, A. C. Vandaele, J. Vander Auwera, J. Quant. Spectroscop. Radiat. Trans. 112 (2011) 2395–2445.

[32] L. S. Rothman, I. E. Gordon, Y. Babikov, A. Barbe, D. Chris Benner, P. F. Bernath, M. Birk, L. Bizzocchi, V. Boudon, L. R. Brown, A. Campargue, K. Chance, E. A. Cohen, L. H. Coudert, V. M. Devi, B. J. Drouin, A. Fayt, J. M. Flaud, R. R. Gamache, J. J. Harrison, J. M. Hartmann, C. Hill, J. T. Hodges, D. Jacquemart, A. Jolly, J. Lamouroux, R. J. Le Roy, G. Li, D. A. Long, O. M. Lyulin,

C. J. Mackie, S. T. Massie, S. Mikhailenko, H. S. P. Müller, O. V. Naumenko, A. V. Nikitin, J. Orphal, V. Perevalov, A. Perrin, E. R. Polovtseva, C. Richard, M. A. H. Smith, E. Starikova, K. Sung, S. Tashkun, J. Tennyson, G. C. Toon, V. G. Tyuterev, G. Wagner, J. Quant. Spectrosc. Radiat. Trans. 130 (2013) 4–50.

[33] Y. L. Babikov, S. N. Mikhailenko, A. Barbe, V. G. Tyuterev, J. Quant. Spectroscop. Radiat. Trans. 145 (2014) 169–196.

[34] Y. Té, P. Jeseck, S. Payan, I. Pepin, C. Camy-Peyret, Rev. Sci. Instr. 81 (2010) 103102.

[35] L. S. Rothman, C. P. Rinsland, A. Goldman, S. T. Massie, D. P. Edwards, J. M. Flaud, A. Perrin, C. Camy-Peyret, V. Dana, J. Y. Mandin, J. Schroeder, A. McCann, R. R. Gamache, R. B. Wattson, K. Yoshino, K. V. Chance, K. W. Jucks, L. R. Brown, V. Nemtchinov, P. Varanasi, J. Quant. Spectroscop. Radiat. Trans. 60 (1998) 665–710.

[36] T. B. Coplen, J. K. Böhlke, P. De Bièvre, T. Ding, N. E. Holden, J. A. Hopple, H. R. Krouse, A. Lamberty, H. S. Peiser, K. Révész, S. E. Rieder, K. J. R. Rosman, E. Roth, P. D. P. Taylor, R. D. Vocke, Y. K. Xiao, Pure Appl. Chem. 74 (2002) 1987–2017.

[37] C. A. M. Brenninkmeijer, C. Janssen, J. Kaiser, T. Röckmann, T. S. Rhee, S. S. Assonov, Chem. Rev. 103 (2003) 5125–5161.

[38] D. Krankowsky, P. Lämmerzahl, K. Mauersberger, C. Janssen, B. Tuzson, T. Röckmann, J. Geophys. Res. 112 (2007) D08301.

[39] A. M. Goldman, F. J. Murcray, D. G. Murcray, J. J. Kosters, C. P. Rinsland, J. M. Flaud, C. Camy-Peyret, A. Barbe, J. Geophys. Res. 94 (1989) 8467–8473.

[40] J.-M. Flaud, C. Piccolo, P. Cali, A. Perrin, L. H. Coudert, J.-L. Teffo, L. R. Brown, Atmos. Oceanic Opt. 16 (2003) 172 – 182.

[41] J. Flaud, C. Camy-Peyret, C. P. Rinsland, M. A. H. Smith, V. M. Devi, Atlas of ozone spectral parameters from microwave to medium infrared, Academic Press Inc., Boston, 1990.

[42] A. Barbe, J. J. Plateaux, S. Bouazza, O. Sulakshina, S. Mikhailenko, V. Tyuterev, S. Tashkun, J. Quant. Spectroscop. Radiat. Transfer 52 (1994) 341–355.

[43] A. Barbe, V. G. Tyuterev, 2013. Pers. communication.

[44] F. Hase, J. W. Hannigan, M. T. Coffey, A. Goldman, M. Hopfner, N. B. Jones, C. P. Rinsland, S. W. Wood, J. Quant. Spectroscop. Radiat. Trans. 87 (2004) 25–52.

[45] S. A. Clough, M. W. Shephard, E. J. Mlawer, J. S. Delamere, M. J. Iacono, K. Cady-Pereira, S. Boukabara, P. D. Brown, J. Quant. Spectroscop. Radiat. Trans. 91 (2005) 233–244.

[46] F. Hase, Atmos. Meas. Tech. 5 (2012) 603–610.

[47] F. Hase, T. Blumenstock, C. Paton-Walsh, Appl. Opt. 38 (1999) 417–3422.

[48] M. Schneider, F. Hase, Atmos. Chem. Phys. 8 (2008) 63–71.

[49] A. Laeng, U. Grabowski, T. von Clarmann, G. Stiller, N. Glatthor, M. Hopfner, S. Kellmann, M. Kiefer, A. Linden, S. Lossow, Atmos. Meas. Tech. 7 (2014) 3971–3987.

[50] R. Lindenmaier, R. L. Batchelor, K. Strong, H. Fast, F. Goutail, F. Kolonjari, C. T. McElroy, R. L. Mittermeier, K. A. Walker, J. Quant. Spectroscop. Radiat. Transfer 111 (2009) 569–585.

[51] H. Tran, F. Rohart, C. Boone, M. Eremenko, F. Hase, P. Bernath, J. M. Hartmann, J. Quant. Spectrosc. Radiat. Trans. 111 (2010) 2012–2020. doi:10.1016/j.jqsrt.2010.04.002.

[52] H. Tran, B. Picquet-Varrault, C. Boursier, C. Viatte, M. Eremenko, F. Hase, J. M. Hartmann, J. Quant. Spectrosc. Radiat. Trans. 112 (2011) 2287–2295. doi:10.1016/j.jqsrt.2011.06.001.

Table 1: Technical data of the Paris-FTS and supporting instruments situated at 48° 50′N, 22° 1′E at 60 m above sea level

| | |
|---|---|
| *FTS* | |
| Instrument Model | IFS 125HR |
| Max. opt. path difference | 258 cm |
| Spectral resolution | $2.4 \cdot 10^{-3}$ cm$^{-1}$ |
| Nominal beam diameter | 63.5 mm |
| Focal length | 418 mm |
| Field stop aperture | 1 mm |
| Instrument vacuum | < 1 Pa |
| 10 µm range | MCT detector |
| | KBr beam splitter |
| Filter transmission ($T_F$) | $T_F$(centre) > 60 % |
| | $T_F$(50 %) cut on @ 7.14 µm |
| | $T_F$(50 %) cut off @ 10.0 µm |
| 4.8 µm range | InSb detector |
| | KBr beam splitter |
| Filter transmission ($T_F$) | $T_F$(centre) > 60 % |
| | $T_F$(50 %) cut on at 3.3 µm |
| | $T_F$(50 %) cut off at 5.0 µm |
| Duration of acquisition | 3 min (2 co-adds) |
| Acquisition dates | 2013-07-19; 2013-07-20; |
| | 2013-07-22; 2013-08-16; |
| | 2013-08-21; 2013-08-23; |
| *Sun Tracker* | |
| Model | Bruker A547 |
| Pointing precision | 1 arc min. (8h) |

Table 2: Global comparison of spectroscopic parameters contained in the databases. Two symbols indicate availability of the data in both the 5 and 10 μm windows, respectively. + or − signs mean that values are provided or not provided. Symbols O and F indicate that values have been set to zero or to another fixed standard value, and X signifies that only a few lines have values different from the standard value.

| Parameter | Symbol | G11 | H12 | S15 |
|---|---|---|---|---|
| (Vacuum wavenumber) position | $\nu$ | +/+ | +/+ | +/+ |
| Intensity | $S\,(296\,\mathrm{K})$ | +/+ | +/+ | +/+ |
| Lower-state energy (as wavenumber) | $E''$ | +/+ | +/+ | +/+ |
| Air (broadened half) width | $\gamma_{\mathrm{air}}$ | +/+ | +/+ | +/+ |
| Self (broadened half) width | $\gamma_{\mathrm{self}}$ | +/+ | +/+ | +/+ |
| Air (pressure induced) shift | $\delta_{\mathrm{air}}$ | O/O | X/X | −/− |
| Temperature (dependence) exponent (for $\gamma_{\mathrm{air}}$) | $n_{\mathrm{air}}$ | F/F | +/+ | −/− |

Table 3: Spectral windows for the retrieval of total $O_3$ columns ($C_{O_3}$) based on the H12 database

| Spectral window | Overall spectral range ($cm^{-1}$) | Micro-window ($cm^{-1}$) | Effective window width ($cm^{-1}$) | No of $O_3$ lines above threshold / total | Interfering species |
|---|---|---|---|---|---|
| 10−1 | 991.25 − 1013.19 | 991.250 − 993.800 | 9.440 | 666: 854/3470 | $H_2O$, $CO_2$, $C_2H_4$ |
| | | 1001.470 −1003.040 | | 668: 169/ 421 | |
| | | 1005.000 −1006.900 | | 686: 109/ 264 | |
| | | 1007.470 −1008.900 | | 667: 5/ 289 | |
| | | 1011.200 −1013.190 | | 676: 20/ 143 | |
| 5−1 | 2070.90 − 2084.64 | 2070.900 −2071.113 | 3.193 | 666: 166/1452 | $H_2O$, $CO_2$, CO, OCS |
| | | 2079.600 −2080.500 | | | |
| | | 2080.960 −2081.500 | | | |
| | | 2082.500 −2083.700 | | | |
| | | 2084.300 −2084.640 | | | |
| 5−2 | 2101.15 − 2109.90 | 2101.150 −2102.700 | 3.110 | 666: 193/ 577 | $H_2O$, $CO_2$, CO, OCS |
| | | 2103.800 −2104.150 | | | |
| | | 2104.900 −2105.040 | | | |
| | | 2108.830 −2109.900 | | | |
| 5−3 | 2118.40 − 2127.05 | 2118.400 −2118.550 | 2.300 | 666: 105/ 279 | $H_2O$, $CO_2$, CO, OCS |
| | | 2119.900 −2121.000 | | | |
| | | 2122.070 −2122.250 | | | |
| | | 2123.140 −2123.440 | | | |
| | | 2125.470 −2125.700 | | | |
| | | 2126.570 −2126.690 | | | |
| | | 2126.830 −2127.050 | | | |
| 5−4 | 2130.38 − 2134.90 | 2130.380 −2130.490 | 0.750 | 666: 32/ 133 | $H_2O$, $CO_2$, CO, OCS |
| | | 2130.650 −2130.750 | | | |
| | | 2132.440 −2132.780 | | | |
| | | 2134.700 −2134.900 | | | |

Table 4: Sensitivity of the total ozone column $C_{O_3}$. $\alpha$-coefficients (eqs. (5) and (A.1)) indicate the response of $C_{O_3}$ on global relative changes in line intensity ($S$), air broadening ($\gamma_{air}$) and temperature dependence of the air broadening ($n_{air}$) as a function of the vibrational band. Weights have been evaluated at $T = 235$ K.

| Band | Weight $w_I$ (%) | $\alpha(x)$ or $\alpha_I(x)$ | | | $\alpha(\gamma_{air})/\alpha(n_{air})$ | $-\alpha(\gamma_{air})/\alpha(S)$ | $-\alpha(n_{air})/\alpha(S)$ |
|---|---|---|---|---|---|---|---|
| | | $x = S$ | $x = \gamma_{air}$ | $x = n_{air}$ | | | |
| 001 ← 000 | 91.2 | −0.94 | −0.152 | −0.049 | 3.3 | −0.163 | −0.048 |
| 011 ← 010 | 5.0 | −1.75 | 0.541 | 0.063 | 5.3 | 0.310 | 0.056 |
| 100 ← 000 | 1.7 | −0.86 | 0.245 | 0.021 | 5.6 | 0.286 | 0.050 |
| 002 ← 001 | 1.5 | −1.51 | 0.286 | 0.067 | 4.3 | 0.273 | 0.064 |
| Weighted sum | 99.4 | −0.98 | −0.104 | −0.035 | 3.0 | −0.126 | −0.040 |

Table 5: Relative deviations ($x_{H12}/x_{G11} - 1$ and $x_{H12}/x_{S15} - 1$) of intensity weighted spectral parameters $x$ in the H12, G11 and S15 databases, restricted to the observational window 10–1 at 10 μm. Differences are given separately for the main ($^{16}O_3$) and the rare $^{18}O$-containing isotopes.

| Band | $(x_{H12}/x_{G11} - 1)$ (%) | | | $(x_{H12}/x_{S15} - 1)$ (%) | |
|---|---|---|---|---|---|
| | $x = S$ | $x = \gamma_{air}$ | $x = n_{air}$ | $x = S$ | $x = \gamma_{air}$ |
| | | | $^{16}O_3$ | | |
| all | 0.21 | 1.15 | 1.10 | 0.07 | 1.85 |
| 001 ← 000 | 0.06 | 0.35 | 1.28 | 0.02 | 1.50 |
| 011 ← 010 | −1.57 | 13.28 | −0.84 | −0.77 | 4.73 |
| 100 ← 000 | 0.06 | 0.25 | 5.63 | −0.42 | 3.14 |
| 002 ← 001 | −3.85 | 7.46 | −5.77 | −1.41 | 7.46 |
| | | | $^{16}O^{16}O^{18}O$ | | |
| all | −3.85 | 3.93 | −3.74 | −0.61 | −0.13 |
| 001 ← 000 | −3.85 | 3.91 | −3.84 | −2.25 | 0.01 |
| | | | $^{16}O^{18}O^{16}O$ | | |
| all | −3.85 | 10.17 | −6.29 | −0.84 | 10.23 |
| 001 ← 000 | −3.85 | 10.18 | −6.30 | −2.83 | 10.21 |

Table 6: Relative deviations $\Delta S/S|_{\mathrm{H-G}} = (S_{\mathrm{H12}}/S_{\mathrm{G11}} - 1)$ and $\Delta S/S|_{\mathrm{H-S}} = (S_{\mathrm{H12}}/S_{\mathrm{S15}} - 1)$ of intensity weighted intensities at 235 K in the H12, G11 and S15 databases, restricted to the observational windows 5−1 and 5−2 to 5−4 at 5 μm.

| Band | 5−1 | | | 5−2 to 5−4 | | |
|---|---|---|---|---|---|---|
| | Weight (%) | $\Delta S/S\|_{\mathrm{H-G}}$ (%) | $\Delta S/S\|_{\mathrm{H-S}}$ (%) | Weight (%) | $\Delta S/S\|_{\mathrm{H-G}}$ (%) | $\Delta S/S\|_{\mathrm{H-S}}$ (%) |
| all | 100.0 | −2.7 | −0.6 | 100.0 | −4.1 | −2.6 |
| 101 ← 000 | 86.3 | −2.6 | −0.3 | 96.3 | −4.0 | −2.5 |
| 002 ← 000 | 10.9 | −0.8 | 6.1 | 3.1 | 0.2 | 3.2 |
| 111 ← 010 | 2.5 | 0.0 | 0.0 | 0.4 | 0.0 | 0.0 |
| 200 ← 000 | 0.3 | 0.0 | 0.0 | 0.2 | 2.9 | 7.9 |

Highlights

- Present simple method of spectral database comparison based on weighted intensities
- Analyze ozone spectral data in the 5 and 10 μm ranges using ground based FTIR
- Compare GEISA2011, HITRAN2012 and S&MPO2015 databases using total ozone columns
- All databases are consistent within ±2% when comparing 5 and 10 μm regions

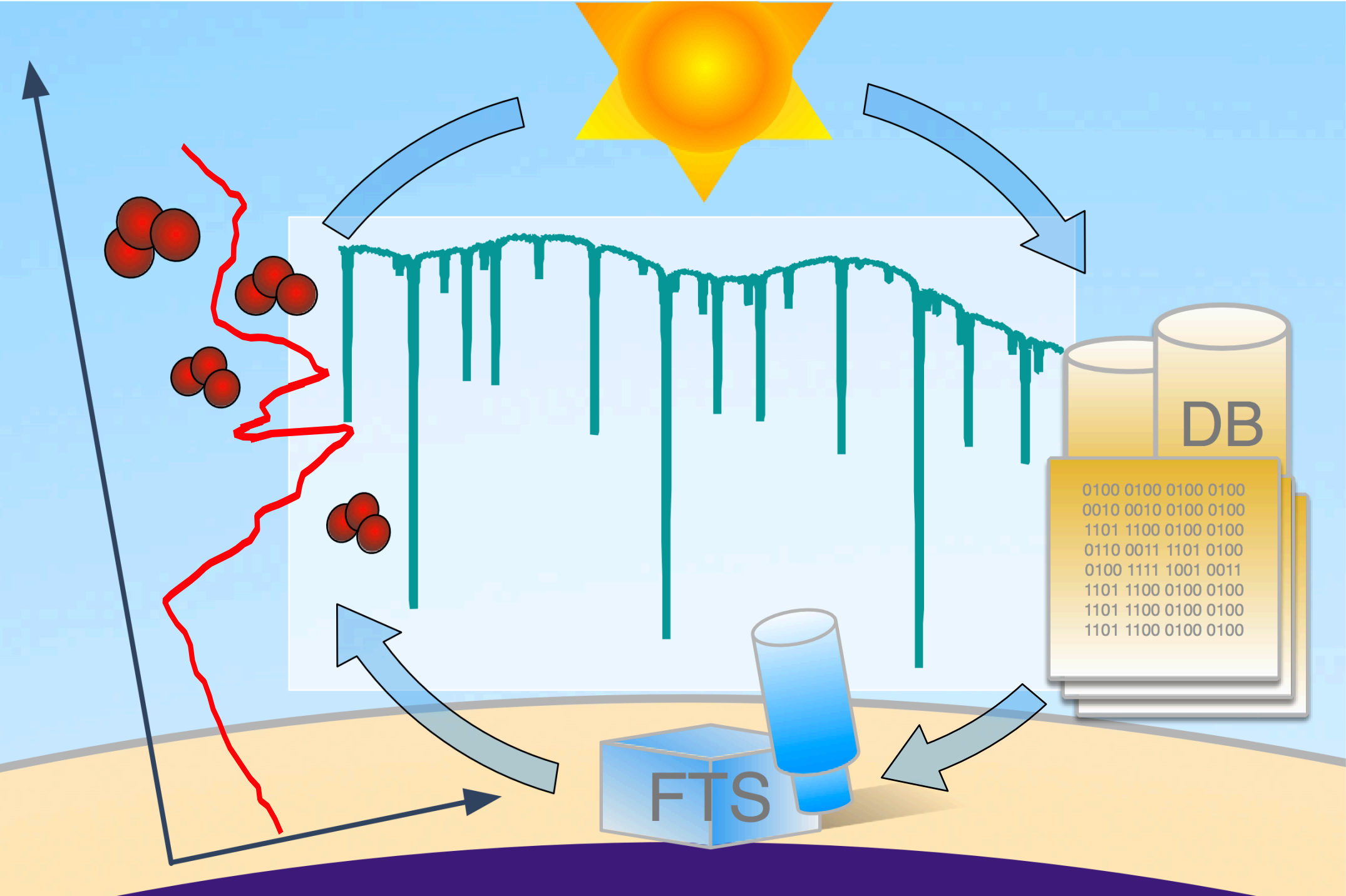
DB
0100 0100 0100 0100
0010 0010 0100 0100
1101 1100 0100 0100
0110 0011 1101 0100
0100 1111 1001 0011
1101 1100 0100 0100
1101 1100 0100 0100
1101 1100 0100 0100
FTS